A Semianalytical Gradient Model for Characterization of Conductors With Surface Roughness

Liang Chen, *Student Member, IEEE*, Min Tang, *Member, IEEE*, and Junfa Mao, *Fellow, IEEE*

***Abstract*— In this paper, a novel semianalytical gradient model (SAGM) for characterizing conductors with surface roughness is presented. Based on the linear function of conductivity, the governing equation of the magnetic field is reduced to the modified Bessel equation, which has an analytical solution. With the piecewise linear approximation technique, the SAGM is derived to deal with arbitrary functions of conductivity. Three typical distributions, including the uniform, normal, and Rayleigh distributions, are investigated. The proposed SAGM is employed to evaluate the propagation properties of typical transmission line structures with different surface roughness profiles. The simulation results agree well with those from measurements, which confirm the validity and accuracy of the proposed method.**

***Index Terms*— Attenuation constant, conductor surface roughness, effective conductivity, semianalytical gradient model (SAGM), transmission line.**

I. Introduction

With the rapid increase in operating frequencies and continuous decrease in geometric dimensions of microwave circuits, the propagation performance of transmission lines is becoming more and more important [1]. With the assumption of smooth conductors, the variation of distributed resistance of transmission line is inversely proportional to the square root of the frequency due to the well-known skin effect. In reality, however, the copper surfaces are intentionally roughened to promote adhesion to the dielectric when manufacturing printed circuit boards (PCBs). The resulting copper surfaces hold a "saw tooth"-like structure. When the tooth height is comparable to the skin depth, the smooth copper assumptions break down [2]. The main reason is that the existence of surface roughness on a conductor disturbs current flow and induces the additional components of ohmic loss. Thus, at high frequencies, the surface roughness will increase the loss of transmission line significantly. Therefore, it is essential to characterize the conductor surface roughness and account for its impact for accurate modeling of transmission structures [3].

In the last decades, the effects of surface roughness on the electrical performance of transmission structures have been investigated in many research works. Some empirical and analytical formulas for modeling conductor surface roughness have been proposed [4]–[9]. For instance, the widely known Hammerstad model, which is based on the assumption of periodic "tooth structure," has been developed in [5]. A correction factor is utilized to account for additional loss due to roughness. However, the major limitation of the Hammerstad model is that it is only suitable for low frequencies or low values of root-mean-square (rms) roughness, because the correction factors saturate at a maximum value of 2, which leads to the lack of accuracy at high frequencies.

The hemispherical model [6] is an improvement over the Hammerstad model. As an approximation of "tooth structure," a hemispherical boss sitting on a plane is chosen to represent the individual surface protrusions. However, when the frequency increases over 30 GHz, the underestimation of loss becomes apparent. The Huray model [7], [8] is developed from the hemispherical model, where the surface roughness is modeled as a pyramidal stack-up of spherical conductor particles snowballs on a conductor surface. The total loss of the structure is calculated based on the superposition of the sphere losses. Besides the traditional planar transmission lines, such as microstrip and stripline, the surface roughness modeling for substrate-integrated waveguide (SIW) has also been investigated [9]. The modified Huray model and rigorous waveguide model are proposed to take into account the mode-dependent loss. Nevertheless, it is difficult to obtain the snowball dimensions and the number of spheres in each protrusion.

Recently, based on the extraction of roughness parameters and electromagnetic field theory, a gradient model for treating surface roughness is proposed [10], [11]. The standard deviation of the surface profile is utilized as a single parameter in the modeling. This model is capable to predict the roughness impact on loss and phase delay in typical transmission lines at high frequencies, even up to 100 GHz. Nevertheless, unlike the traditional empirical models, it involves complicated numerical computation with the finite-difference method (FDM) [12] in the modeling process, which is not convenient in the engineering applications. In order to overcome this problem, an analytical gradient model (AGM) [13] is presented to characterize the conductor surface roughness in our previous

Manuscript received May 1, 2018; revised July 31, 2018; accepted August 29, 2018. Date of publication October 15, 2018; date of current version December 11, 2018. This work was supported in part by the Science Challenge Project under Grant TZ2018003 and in part by the National Natural Science Foundation of China under Grant 61674105 and Grant 61331004. This paper is an expanded version from the IEEE MTT-S International Microwave Symposium (IMS), June 10–15, 2018, Philadelphia, PA, USA. *(Corresponding author: Min Tang.)*

The authors are with the Key Laboratory of Ministry of Education of China for Research of Design and Electromagnetic Compatibility of High Speed Electronic Systems, Shanghai Jiao Tong University, Shanghai 200240, China (e-mail: tm222@sjtu.edu.cn).

Color versions of one or more of the figures in this paper are available online at http://ieeexplore.ieee.org.

Digital Object Identifier 10.1109/TMTT.2018.2873351

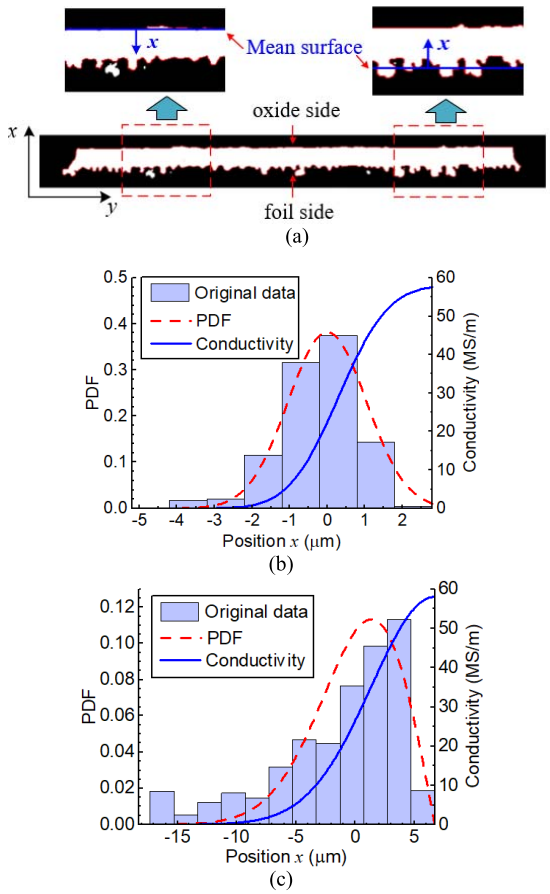

Fig. 1. (a) Microscope image of a rough conductor (including enlarged photograph for details) with (b) normal distribution on the oxide side and (c) Rayleigh distribution on the foil side. The PDFs and corresponding position-dependent conductivities are also illustrated.

work. The AGM is derived based on the uniform distribution function for the random rough surface. This analytical model is then implemented to investigate the impact of surface roughness on both the electrical and thermal performances of microstrip lines.

In this paper, a novel semi-AGM (SAGM) is proposed to characterize conductors with surface roughness. Three typical distributions, including the uniform, normal, and Rayleigh distributions, are introduced to describe the surface roughness of copper foils. Using the piecewise linear approximation scheme, the SAGM is developed to handle rough conductors with arbitrary position-dependent functions of conductivities. In applications, the proposed SAGM is utilized to achieve attenuation constants of striplines with different surface roughness profiles. The simulation results are consistent with the measurements. In addition, the propagation properties of SIWs are also evaluated with the SAGM.

II. SAGM

In this section, a systematic approach based on the SAGM is developed to achieve the effective conductivity of conductors with surface roughness.

With the probability theory and statistics, the surface roughness of copper conductor can be characterized by certain distribution functions. For instance, a copper foil conductor has two parallel surfaces, which are named as "foil side" and "oxide side," respectively, as shown in Fig. 1(a) [14]. By extracting the conductor roughness profile, it is obtained that the surface roughness on the foil side satisfies the normal distribution, while that on the oxide side belongs to the Rayleigh distribution, as depicted in Fig. 1(b) and (c) [14] respectively. Thus, the probability density functions (PDFs) of finding a point at a distance x from the mean surface can be described by the normal and Rayleigh distributions, respectively. According to the statistical representation, the corresponding cumulative distribution functions (CDFs) are provided in Appendix I.

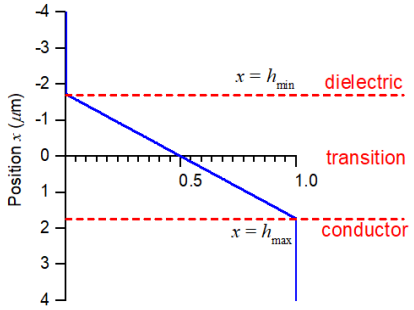

Fig. 2. Normalized linear function of conductivity in the transition region.

Since the conductivity $\sigma(x)$ of a conductor with surface roughness is proportional to CDF(x), when the CDF parameter is determined, the position-dependent conductivity is readily obtained by [10]

$$\sigma(x) = \sigma_{\mathrm{dc}}\mathrm{CDF}(x) \tag{1}$$

where σ_{dc} is the dc conductivity. For illustration, the characteristics of $\sigma(x)$ for both the normal and Rayleigh distributions are also described in Fig. 1.

Then, in order to achieve the governing equation for predicting the loss for a rough conductor, it is assumed that only a normal component of the electric field ($\mathbf{E}_{\perp}$) and a tangential component of the magnetic field ($\mathbf{B}_{||}$) exist outside the conductor. Thus, the original 3-D problem can be reduced to a 1-D one. The resulting governing equation of the magnetic field is given by [10]

$$\frac{\partial^2}{\partial x^2}\mathbf{B}_{||} - j\omega\mu\sigma(x)\mathbf{B}_{||} - \frac{\partial}{\partial x}\ln\sigma(x)\frac{\partial}{\partial x}\mathbf{B}_{||} = 0. \tag{2}$$

Note that the third term on the left-hand side of (2) originates from the position-dependent conductivity $\sigma(x)$. If the conductivity is constant, (2) is simplified to the classical Helmholtz equation for describing the high-frequency effects of conductors with smooth surfaces.

A. Analytical Solution for Linear Conductivity

First, the position-dependent conductivity perpendicular to the conductor surface is expressed by a linear function in the transition region between dielectric and conductor (see Fig. 2), as

$$\sigma(x) = \sigma_{\mathrm{dc}}k(x+q) \quad h_{\min} \le x \le h_{\max} \tag{3}$$

where k and q are the two constants, $h_{\max}$ and $h_{\min}$ are the up and down boundaries of the transition, respectively.

The normalized form of (3) is illustrated in Fig. 2, where the value in dielectric region is 0, and that in conductor region is 1.

Therefore, the specific solution of (2) is related to different regions. First, in the region of $h_{\min} < x < h_{\max}$, (2) can be expressed as

$$(x+q)^2\frac{\partial^2}{\partial x^2}\mathbf{B}_{||} - (x+q)\frac{\partial}{\partial x}\mathbf{B}_{||} - j\omega\mu\sigma_{\rm dc}k(x+q)^3\mathbf{B}_{||} = 0. \tag{4}$$

With the elementary transformations of the dependent and independent variables [15], (4) can be simplified as a classical Bessel's equation

$$x^2\frac{d^2y}{dx^2} + x\frac{\partial y}{\partial x} + (x^2 - p^2)y = 0. \tag{5}$$

The detailed derivation is described in Appendix II.

Then, the analytical solution of (4) is given by

$$\mathbf{B}_{||}(x) = A(x+q)I_{2/3}(\Theta) + B(x+q)K_{2/3}(\Theta) \tag{6}$$

where A and B are the two constant coefficients to be determined, $I_{2/3}(\Theta)$ and $K_{2/3}(\Theta)$ are the two-third-order modified Bessel functions of the first and second kinds, respectively, and Θ is calculated by

$$\Theta = j^{\frac{1}{2}}\frac{2\sqrt{\omega\mu\sigma_{\rm dc}k}}{3}(x+q)^{3/2}. \tag{7}$$

Accordingly, the derivative of the magnetic field is obtained by

$$\frac{d}{dx}\mathbf{B}_{||}(x) = A\left(2I_{2/3}(\Theta) + \frac{2}{3}\Theta I_{5/3}(\Theta)\right) + B\left(2K_{2/3}(\Theta) - \frac{2}{3}\Theta K_{5/3}(\Theta)\right). \tag{8}$$

Second, due to the fact that the third term in (2) comes from the position-dependent conductivity, it will disappear in the region of $x > h_{\max}$, and (2) becomes the well-known Helmholtz equation describing the classical skin effect in ideally smooth surfaces

$$\frac{\partial^2}{\partial x^2}\mathbf{B}_{||} - j\omega\mu\sigma\mathbf{B}_{||} = 0. \tag{9}$$

The analytical solution is written as

$$\mathbf{B}_{||}(x) = C \times \exp\left[-(1+j)\frac{x}{\delta}\right] \tag{10}$$

where C is another unknown constant, and δ is the skin depth

$$\delta = \sqrt{\frac{2}{\omega\mu\sigma}}. \tag{11}$$

Similarly, the derivative of the magnetic field is

$$\frac{d}{dx}\mathbf{B}_{||}(x) = -\frac{(1+j)C}{\delta}\exp\left[-(1+j)\frac{x}{\delta}\right]. \tag{12}$$

At the interface of $x = h_{\max}$, the magnetic field and its derivation should be continuous. Thus, we have

$$\mathbf{B}_{||}(h_{\max})^- = \mathbf{B}_{||}(h_{\max})^+ \tag{13}$$

$$\frac{d\mathbf{B}_{||}(h_{\max})^-}{dx} = \frac{d\mathbf{B}_{||}(h_{\max})^+}{dx}. \tag{14}$$

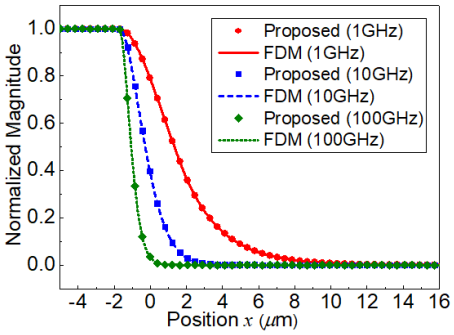

Fig. 3. Normalized magnitude of the magnetic field for linear conductivity case.

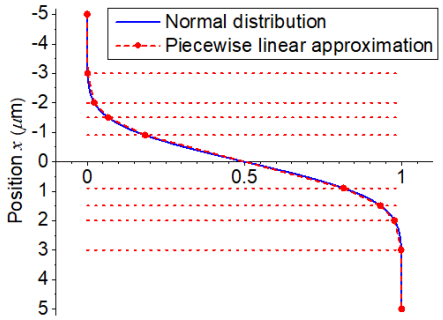

Fig. 4. Normalized piecewise linear function of conductivity in the transition region.

According to the above relations and assuming that $\mathbf{B}_{||}$ is normalized to unity at $x = h_{\min}$, the values of constants A, B, and C in (6) and (10) can be determined.

To validate the above-mentioned model, the magnetic field parallel to a rough copper surface is investigated. Without loss of generality, the rms of conductor surface roughness is set to 1 μm. The normalized amplitudes of magnetic fields are calculated by the proposed method, and compared with those from FDM in [10]. As observed in Fig. 3, the results of two approaches are in very good agreement for different operating frequencies. Since the proposed method is based on the analytical formulas, it holds inherent advantages in computational efficiency and provides accurate results as well.

B. Semianalytical Solution for Arbitrary Conductivity

In real applications, however, the expressions of position-dependent conductivities may be much more complicated than a linear function. Therefore, it is difficult to derive an analytical solution of (2) directly. To conquer this problem, the piecewise linear approximation is utilized for the derivation of SAGM.

For instance, the curve of Gaussian-CDF can be approximated by a group of piecewise linear sections, as shown in Fig. 4. The resulting conductivity is expressed as

$$\sigma(x) = \sigma_{\rm dc} \times \begin{cases} 0, & x < x_0 \\ k_1(x+q_1), & x_0 \le x < x_1 \\ \dots & \\ k_N(x+q_N), & x_{N-1} \le x < x_N \\ 1, & x_N \le x. \end{cases} \tag{15}$$

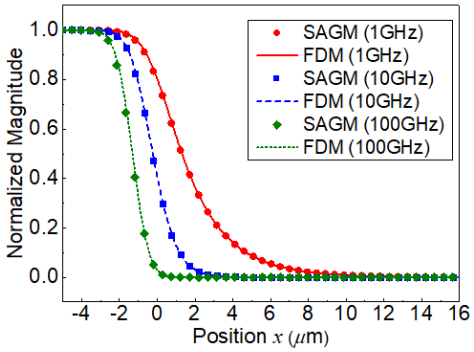

Fig. 5. Normalized magnitude of the magnetic field for arbitrary conductivity case.

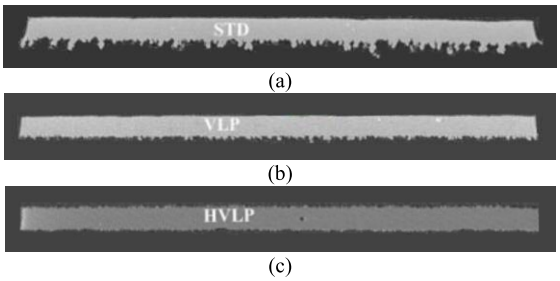

Fig. 6. SEM photograph of signal traces for (a) STD, (b) VLP, and (c) HVLP.

Similar to the procedure in Section II-A, for a section of $x_{n-1} \le x < x_n$ $(n = 1, 2, \ldots, N-1)$, the analytical solution of the magnetic field is

$$\mathbf{B}_{||}(x)|_n = A_n(x+q_n)I_{2/3}(\Theta_n) + B_n(x+q_n)K_{2/3}(\Theta_n) \quad (16)$$

where A_n and B_n are the constant coefficients to be determined, and Θ_n is calculated by

$$\Theta_n = j^{\frac{1}{2}}\frac{2\sqrt{\omega\mu\sigma_{\rm dc}k_n}}{3}(x+q_n)^{3/2}. \quad (17)$$

Based on the continuity requirements [similar to (13) and (14)] for the magnetic field and its derivative at each interface, we will finally obtain a matrix equation as

$$\mathbf{Ax} = \mathbf{b} \quad (18)$$

where

$$\mathbf{x} = [B_1 \quad A_1 \quad \ldots \quad \ldots \quad B_N \quad A_N \quad C]^T$$
$$\mathbf{b} = [1 \quad 0 \quad \ldots \quad \ldots \quad 0 \quad 0 \quad 0]^T$$

and $\mathbf{A}$ is a $(2N+1)\times(2N+1)$ matrix described in (19), shown at the bottom of the next page.

At the first interface, the element in A is

$$a_{11} = (x+q_1)K_{2/3}(\Theta_1)|_{x=x_0}.$$

For the nth interface in the middle region, the corresponding elements are given by

$$\begin{aligned}
a_{(2n)(2n-1)} &= (x+q_n)K_{2/3}(\Theta_n)|_{x=x_n}\\
a_{(2n)(2n)} &= (x+q_n)I_{2/3}(\Theta_n)|_{x=x_n}\\
a_{(2n)(2n+1)} &= -(x+q_{n+1})K_{2/3}(\Theta_{n+1})|_{x=x_n}\\
a_{(2n)(2n+2)} &= -(x+q_{n+1})I_{2/3}(\Theta_{n+1})|_{x=x_n}\\
a_{(2n+1)(2n-1)} &= \left[2K_{2/3}(\Theta_n) - \frac{2}{3}\Theta_n K_{5/3}(\Theta_n)\right]\Big|_{x=x_n}
\end{aligned}$$

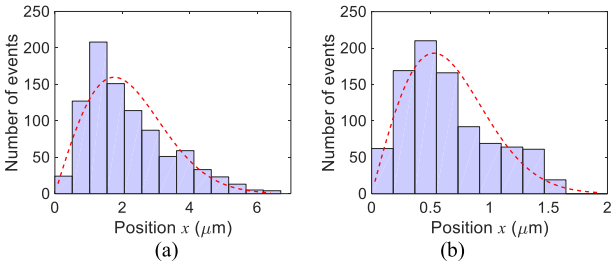

Fig. 7. Height histograms and PDFs of the foil sides for (a) STD and (b) VLP.

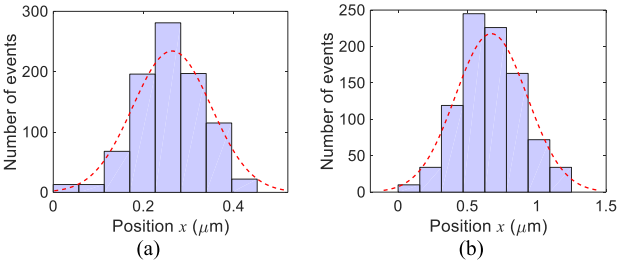

Fig. 8. Height histograms and PDFs for HVLP of (a) oxide side and (b) foil side.

$$\begin{aligned}
a_{(2n+1)(2n)} &= \left[2I_{2/3}(\Theta_n) + \frac{2}{3}\Theta_n I_{5/3}(\Theta_n)\right]\Big|_{x=x_n}\\
a_{(2n+1)(2n+1)} &= \left[-2K_{2/3}(\Theta_{n+1}) + \frac{2}{3}\Theta_{n+1}K_{5/3}(\Theta_{n+1})\right]\Big|_{x=x_n}\\
a_{(2n+1)(2n+2)} &= \left[-2I_{2/3}(\Theta_{n+1}) - \frac{2}{3}\Theta_{n+1}I_{5/3}(\Theta_{n+1})\right]\Big|_{x=x_n}.
\end{aligned}$$

At the last interface, the elements are determined by

$$\begin{aligned}
a_{(2N)(2N+1)} &= -\exp\left[-(1+j)\frac{x}{\delta}\right]\Big|_{x=x_N}\\
a_{(2N+1)(2N+1)} &= \frac{(1+j)}{\delta}\exp\left[-(1+j)\frac{x}{\delta}\right]\Big|_{x=x_N}.
\end{aligned}$$

Note that since the Gaussian-CDF varies drastically at the two ends, the uniform partitioning strategy may induce ill-conditioned matrix $\mathbf{A}$. Thus, appropriate partitioning of regions is important to ensure the accuracy and stability of SAGM. Based on an adaptive scheme, this issue can be solved successfully. In addition, the skin depth varies with operating frequency. Denser partitioning in the region of skin depth is required to guarantee accurate approximation in higher frequency cases.

Similar to the analytical case in Section II-A, the accuracy of the proposed SAGM is also verified by the FDM in [10]. The normalized magnitudes of magnetic fields for different operating frequencies are depicted in Fig. 5. It is obvious that the results of SAGM and FDM agree well with each other.

C. Effective Frequency-Dependent Conductivity

With the y-directional component of $\mathbf{B}_{||}$, the roughness impact on loss can be expressed by an effective frequency-dependent conductivity [10]

$$\sigma_{\rm eff}(\omega) = \frac{\omega}{8\mu_0^3}|B_y(0)|^4\left[\int_{\sigma>0}\frac{|J_{\rm rough}(x)|^2}{2\sigma(x)}dx\right]^{-2} \quad (20)$$

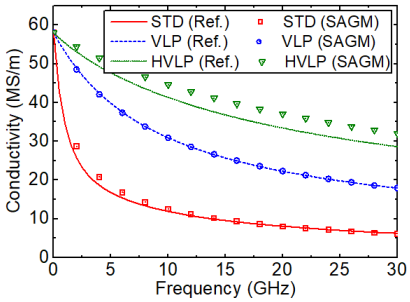

Fig. 9. Effective conductivities for different traces. Those obtained from the original height histograms are represented as "reference."

where the surface current density is

$$J_{\text{rough}}(x) = \frac{1}{\mu}\frac{dB_y(x)}{dx}. \tag{21}$$

For real structures of copper foils, the foil side and oxide side (see Fig. 1) usually hold different roughness parameters. This factor should be taken into account in the derivation of effective conductivity as well. By setting the loss power density of a rough surface equal with that of an ideal smooth surface, we have

$$\int_{\sigma>0}\frac{|J_{\text{smooth}}|^2}{2\sigma_{\text{eff}}}dx = \sum_{i=1}^{N}\frac{L_i}{L}\int_{\sigma>0}\frac{|J_{\text{rough}}(x)|^2}{2\sigma_i(x)}dx \tag{22}$$

where $\sigma_i(x)$ is the position-dependent conductivity of the ith surface, L_i is the profile length of the ith surface, L is the sum of L_i $(i = 1, \ldots, N)$, and N is the total number of surfaces.

III. Application

To demonstrate the validity and accuracy of the proposed SAGM, it is applied to characterize conductor surface roughness and predict propagating properties of two typical microwave transmission line structures in this section.

A. Stripline

In the first example, the traces of stripines with three different foil profiles are investigated. The profiles can be obtained by scanning electron microscope (SEM). As shown in Fig. 6 [16], they are standard (STD), very-low-profile (VLP), and hyper-VLP (HVLP) foils, respectively. The geometrical dimensions and roughness data of them are listed in [16].

By extracting the roughness profiles with SEM [17], we can obtain the height histogram of each trace. As shown in Fig. 7, the foil sides of STD and VLP satisfy the Rayleigh distribution, while the oxide sides of them are relatively smooth to be characterized by the normal distribution. By contrast, both sides of HVLP satisfy the normal distribution, as depicted in Fig. 8.

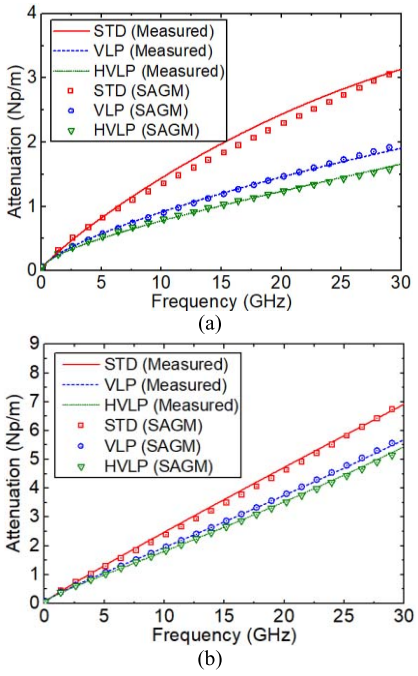

Fig. 10. Simulated and measured attenuation constants for different kinds of traces due to (a) conductor loss and (b) total loss.

The validity for both normal and Rayleigh distributions can be verified by the effective conductivities derived using SAGM. The simulation results are compared in Fig. 9, where those obtained from the original height histograms are indicated as "reference." A good consistency is observed for the STD and VLP cases. The reason for the deviation in the HVLP case is that the roughness height is small, and thus the effective conductivity is sensitive to its profile.

Then, the effective conductivities are utilized for the prediction of attenuation property of striplines with different surface roughness distributions. The attenuation constants of striplines are simulated by the full-wave solver ANSYS HFSS. From Fig. 10, it is seen that the simulated attenuation due to the conductor loss agrees well with the measured one for all three structures. Furthermore, combined with the impact of Dk and Df in dielectric layers [16], the total attenuation constants of

$$\mathbf{A} = \begin{bmatrix} a_{11} & \cdots & 0 & 0 & 0 & 0 & \cdots & 0 & 0 & 0 \\ \vdots & \ddots & \vdots & \vdots & \vdots & \vdots & \ddots & \vdots & \vdots & \vdots \\ 0 & \cdots & a_{(2n)(2n-1)} & a_{(2n)(2n)} & a_{(2n)(2n+1)} & a_{(2n)(2n+2)} & \cdots & 0 & 0 & 0 \\ 0 & \cdots & a_{(2n+1)(2n-1)} & a_{(2n+1)(2n)} & a_{(2n+1)(2n+1)} & a_{(2n+1)(2n+2)} & \cdots & 0 & 0 & 0 \\ \vdots & \ddots & \vdots & \vdots & \vdots & \vdots & \ddots & \vdots & \vdots & \vdots \\ 0 & \cdots & 0 & 0 & 0 & 0 & \cdots & a_{(2N)(2N-1)} & a_{(2N)(2N)} & a_{(2N)(2N+1)} \\ 0 & \cdots & 0 & 0 & 0 & 0 & \cdots & a_{(2N+1)(2N-1)} & a_{(2N+1)(2N)} & a_{(2N)(2N+1)} \end{bmatrix} \tag{19}$$

The first interface

The nth interface

The last interface

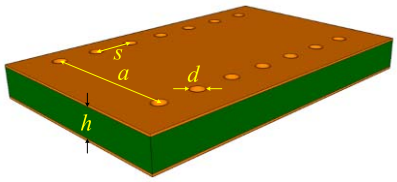

Fig. 11. Schematic of a typical SIW structure with $a = 6.21$ mm, $h = 0.508$ mm, $d = 0.4$ mm, and $s = 0.8$ mm.

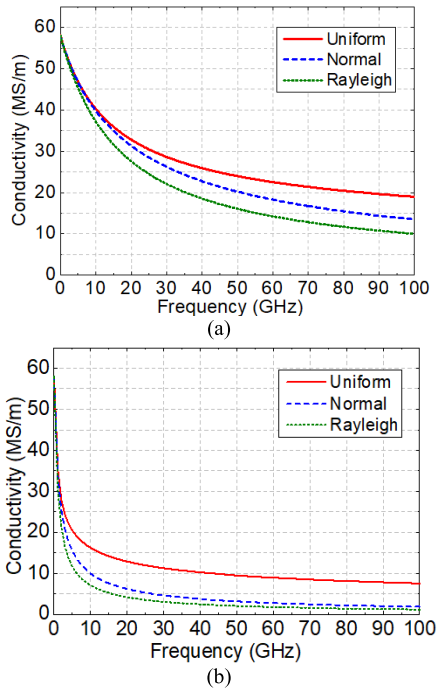

Fig. 12. Effective conductivities for different distribution functions with (a) R_q of 0.25 μm and (b) R_q of 1 μm.

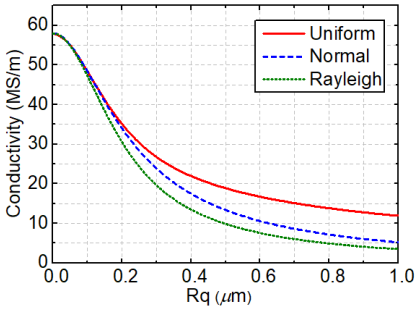

Fig. 13. Effective conductivities with the variation of R_q at 25 GHz.

these striplines are simulated and compared with the measured ones. Again, the excellent agreement is observed.

B. SIW Structure

In the second example, an SIW structure is studied, as shown in Fig. 11. The SIW is designed on Rogers5880 substrate with $\varepsilon_r = 2.2$ and $\tan\delta = 0.0009$. The geometrical parameters of the structure are listed by $a = 6.21$ mm, $h = 0.508$ mm, $d = 0.4$ mm, and $s = 0.8$ mm [18]. According to the waveguide theory, the SIW operates at the middle frequency of 25 GHz for the dominant mode zone.

First, the effective conductivities for three typical distributions (uniform, normal, and Rayleigh) of surface roughness are

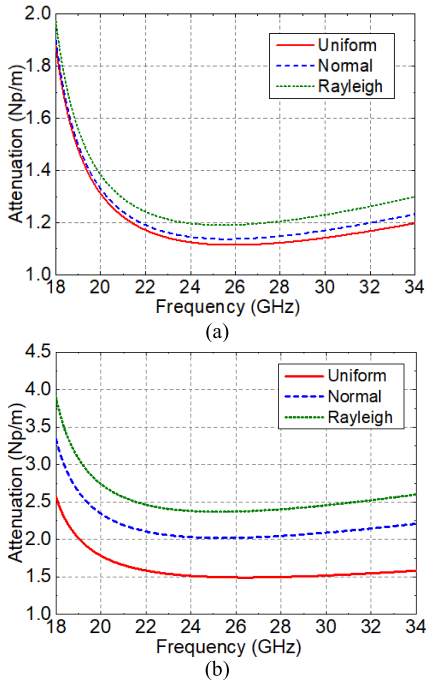

Fig. 14. Attenuation constants for different distribution functions with (a) R_q of 0.25 μm and (b) R_q of 1 μm.

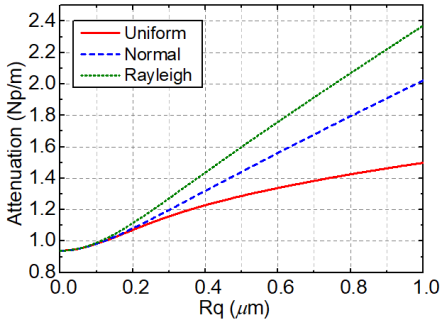

Fig. 15. Attenuation constants with the variation of R_q at 25 GHz.

investigated based on a different R_q (rms value). As shown in Fig. 12, the effective conductivity of the Raleigh distribution is the smallest, while that of uniform distribution is the largest. With the increase of rms roughness from 0.25 to 1 μm, the effective conductivity decreases apparently. It is also observed that the difference between the results of normal and Rayleigh distributions becomes smaller, especially in the high-frequency range. Furthermore, the impact of R_q on effective conductivity at the operating frequency (25 GHz) of SIW is depicted in Fig. 13. We obtain that when R_q is small, the effective conductivities for three distributions are very similar. If R_q is a large value, the results of normal and Rayleigh distributions are close to each other.

Based on the above-mentioned results of effective conductivities, the corresponding attenuation constants of SIWs are compared in Fig. 14. The attenuation constant of the Raleigh distribution is the largest, while that of the uniform distribution is the smallest. From Figs. 14 and 15, we also obtain that the transmission property of SIW will be deteriorated seriously by the rms roughness R_q. Thus, the accurate characterization of surface roughness is essential.

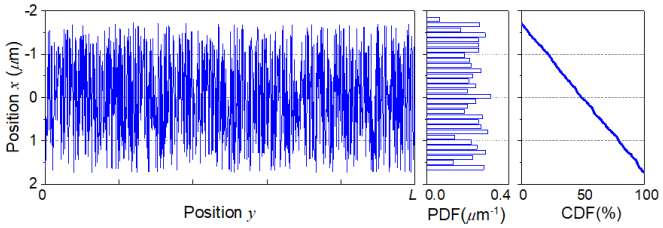

Fig. 16. Relationship between roughness profile, PDF, and CDF for uniform distribution.

IV. Conclusion

In this paper, the SAGM for treating conductor surface roughness with arbitrary distribution functions is presented. Based on the SAGM, a systematic approach is developed to achieve the effective conductivity and evaluate the propagation properties of transmission lines with rough surfaces. The uniform, normal, and Rayleigh distributions are provided as demonstrations. The validity and accuracy of the proposed method are illustrated by evaluating the attenuation constants of typical microwave transmission line structures with different surface roughness profiles. The simulation results agree well with those from measurements.

Appendix I

In this appendix, three typical distributions, including the uniform, normal, and Rayleigh distributions, are introduced to characterize the surface roughness of copper conductors.

A. Uniform Distribution

The continuous uniform distribution is a family of symmetric probability distributions. The PDF of finding a point of height x can be described by

$$\mathrm{PDF}(x) = \begin{cases} \dfrac{1}{h_{\max} - h_{\min}}, & x \in [h_{\min}, h_{\max}] \\ 0, & \text{otherwise} \end{cases} \tag{23}$$

where $h_{\min}$ and $h_{\max}$ are the two boundaries.

With the condition of zero mean, the rms roughness is calculated by

$$R_q = \sqrt{\int_{h_{\min}}^{h_{\max}} x^2 \mathrm{PDF}(x)dx} = \frac{1}{\sqrt{3}}\sqrt{h_{\max}^2 + h_{\max}h_{\min} + h_{\min}^2}. \tag{24}$$

Due to the symmetric probability distribution, we have $h_{\max} = -h_{\min}$, and the rms roughness is

$$R_q = h_{\max}/\sqrt{3} = -h_{min}/\sqrt{3}. \tag{25}$$

The integral function of the PDF is named as CDF, which is given by

$$\mathrm{CDF}(x) = \int_{-\infty}^{x} \mathrm{PDF}(u)du = \begin{cases} 0, & x < h_{\min} \\ \dfrac{x - h_{\min}}{h_{\max} - h_{\min}}, & h_{\min} \le x \le h_{\max} \\ 1, & x > h_{\max}. \end{cases} \tag{26}$$

For clarify, the relationship between roughness profile, PDF, and CDF is shown in Fig. 16.

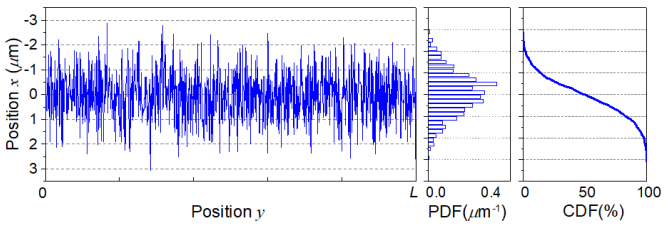

Fig. 17. Relationship between roughness profile, PDF, and CDF for normal distribution.

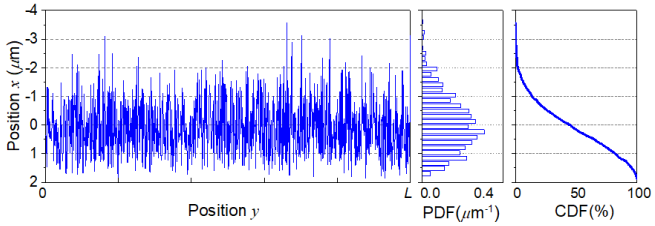

Fig. 18. Relationship between roughness profile, PDF, and CDF for Rayleigh distribution.

B. Normal Distribution

The normal distribution is widely used for describing the surface roughness on the oxide side of copper foils in PCBs, as demonstrated in Fig. 1. The corresponding PDF and CDF parameters are given by

$$\mathrm{PDF}(x) = \frac{1}{R_q\sqrt{2\pi}} \exp\left(-\frac{x^2}{2R_q^2}\right) \tag{27}$$

$$\mathrm{CDF}(x) = \int_{-\infty}^{x} \mathrm{PDF}(u)du = \frac{1}{2}\left[1 + \mathrm{erf}\left(\frac{x}{\sqrt{2}R_q}\right)\right] \tag{28}$$

where $\mathrm{erf}(\cdot)$ represents the Gauss error function, and R_q is the rms roughness.

The relationship between the roughness profile, PDF, and CDF is depicted in Fig. 17.

C. Rayleigh Distribution

The Rayleigh distribution is another important form to characterize the surface roughness on copper foils, especially for the foil side, as shown in Fig. 1. The PDF and CDF parameters for the Rayleigh distribution are expressed as

$$\mathrm{PDF}(h) = -\frac{(4-\pi)\Phi}{2R_q^2} \exp\left[-\frac{(4-\pi)\Phi^2}{4R_q^2}\right] \tag{29}$$

$$\mathrm{CDF}(h) = \int_{-\infty}^{h} \mathrm{PDF}(u)du = \exp\left[-\frac{(4-\pi)\Phi^2}{4R_q^2}\right] \tag{30}$$

where

$$\Phi = h - \sqrt{\frac{\pi}{4-\pi}}R_q \tag{31}$$

and

$$h \le \sqrt{\frac{\pi}{4-\pi}}R_q. \tag{32}$$

Similarly, their characteristics are described in Fig. 18.

APPENDIX II

As a governing equation of the magnetic field, (4) is rewritten here as follows:

$$(x+q)^2\frac{\partial^2}{\partial x^2}\mathbf{B}_{||}-(x+q)\frac{\partial}{\partial x}\mathbf{B}_{||}-j\omega\mu\sigma_{\rm dc}k(x+q)^3\mathbf{B}_{||}=0. \tag{33}$$

It can be transformed into a general form as

$$\bar{x}^2\frac{d^2f}{d\bar{x}^2}+(1-2a)\bar{x}\frac{\partial f}{\partial\bar{x}}-[jb^2c^2\bar{x}^{2c}-(a^2-c^2p^2)]f=0 \quad (p\geq 0, b>0) \tag{34}$$

by setting the following transformation relations:

$$\begin{cases}\bar{x}=x+q\\ a=1,\quad c=3/2\\ b^2c^2=\omega\mu\sigma_{\rm dc}k\\ a^2-c^2p^2=0\end{cases} \tag{35}$$

Then, replacing f by $\bar{x}^a z$, (34) can be written as

$$x^2\frac{d^2z}{dx^2}+x\frac{dz}{dx}-(jb^2c^2x^{2c}+c^2p^2)z=0. \tag{36}$$

Furthermore, using $t=x^c$, we have

$$t^2\frac{d^2z}{dt^2}+t\frac{dz}{dt}-(jb^2t^2+p^2)z=0. \tag{37}$$

After that with $r=j^{1/2}bt$, the modified Bessel equation can be obtained as

$$r^2\frac{d^2z}{dr^2}+r\frac{dz}{dr}-(r^2+p^2)z=0. \tag{38}$$

The analytical solution of (38) is given by [15]

$$f=x^a\left[AI_p\left(j^{\frac{1}{2}}bx^c\right)+BK_p\left(j^{\frac{1}{2}}bx^c\right)\right] \tag{39}$$

where A and B are the two coefficients, $I_p(\cdot)$ and $K_p(\cdot)$ are the first and second kind Bessel functions, respectively.

REFERENCES

[1] R. Achar and M. S. Nakhla, "Simulation of high-speed interconnects," *Proc. IEEE*, vol. 89, no. 5, pp. 693–728, May 2001.

[2] S. H. Hall and H. L. Heck, *Advanced Signal Integrity for High-Speed Digital Designs*. Hoboken, NJ, USA: Wiley, 2009.

[3] L. Tsang, H. Braunisch, R. Ding, and X. Gu, "Random rough surface effects on wave propagation in interconnects," *IEEE Trans. Adv. Packag.*, vol. 33, no. 4, pp. 839–856, Nov. 2010.

[4] S. Groiss, I. Bardi, O. Biro, K. Preis, and K. R. Richter, "Parameters of lossy cavity resonators calculated by the finite element method," *IEEE Trans. Magn.*, vol. 32, no. 3, pp. 894–897, May 1996.

[5] E. Hammerstad and O. Jensen, "Accurate models for microstrip computer-aided design," in *IEEE MTT-S Int. Microw. Symp. Dig.*, Washington, DC, USA, May 1980, pp. 407–409.

[6] S. Hall *et al.*, "Multigigahertz causal transmission line modeling methodology using a 3-D hemispherical surface roughness approach," *IEEE Trans. Microw. Theory Techn.*, vol. 55, no. 12, pp. 2614–2624, Dec. 2007.

[7] P. G. Huray *et al.*, "Fundamentals of a 3-D 'snowball' model for surface roughness power losses," in *Proc. IEEE Workshop Signal Propag. Interconnects*, Genova, Italy, May 2007, pp. 121–124.

[8] P. G. Huray, O. Oluwafemi, J. Loyer, E. Bogatin, and X. Ye, "Impact of copper surface texture on loss: A model that works," *DesignCon*, vol. 1, pp. 462–483, Jun. 2010.

[9] M. Yi *et al.*, "Surface roughness modeling of substrate integrated waveguide in D-band," *IEEE Trans. Microw. Theory Techn.*, vol. 64, no. 4, pp. 1209–1216, Apr. 2016.

[10] G. Gold and K. Helmreich, "A physical surface roughness model and its applications," *IEEE Trans. Microw. Theory Techn.*, vol. 65, no. 10, pp. 3720–3732, Oct. 2017.

[11] G. Gold and K. Helmreich, "Surface impedance concept for modeling conductor roughness," in *IEEE MTT-S Int. Microw. Symp. Dig.*, Phoenix, AZ, USA, May 2015, pp. 1–4.

[12] R. J. L. Veque, *Finite Difference Methods for Ordinary and Partial Differential Equations: Steady-State and Time-Dependent Problems*. Philadelphia, PA, USA: SIAM, 2007.

[13] L. Chen, M. Tang, and J. Mao, "An analytical gradient model for the characterization of conductor surface roughness effects," in *IEEE MTT-S Int. Microw. Symp. Dig.*, Philadelphia, PA, USA, Jun. 2018, pp. 1–4.

[14] M. Koledintseva. *Extraction of Dielectric Properties of PCB Laminated Dielectrics on PCB Striplines Taking Into Account Conductor Surface Roughness*. Accessed: 2018. [Online]. Available: https://ewh.ieee.org/r6/scv/emc/archive/2014/052014Marina.pdf

[15] G. N. Watson, *A Treatise on the Theory of Bessel Functions*. Cambridge, U.K.: Cambridge Univ. Press, 1944.

[16] M. Y. Koledintseva, A. V. Rakov, A. I. Koledintsev, J. L. Drewniak, and S. Hinaga, "Improved experiment-based technique to characterize dielectric properties of printed circuit boards," *IEEE Trans. Electromagn. Compat.*, vol. 56, no. 6, pp. 1559–1566, Dec. 2014.

[17] A. V. Rakov, S. De, M. Y. Koledintseva, S. Hinaga, J. L. Drewniak, and R. J. Stanley, "Quantification of conductor surface roughness profiles in printed circuit boards," *IEEE Trans. Electromagn. Compat.*, vol. 57, no. 2, pp. 264–273, Apr. 2015.

[18] Y. J. Cheng, K. Wu, and W. Hong, "Power handling capability of substrate integrated waveguide interconnects and related transmission line systems," *IEEE Trans. Adv. Packag.*, vol. 31, no. 4, pp. 900–909, Nov. 2008.

Liang Chen (S'16) was born in 1992. He received the B.E. degree in electromagnetic field and wireless technology from Northwestern Polytechnical University, Xi'an, China, in 2015. He is currently pursuing the Ph.D. degree in electronic science and technology at Shanghai Jiao Tong University, Shanghai, China.

His current research interests include signal integrity of high-speed interconnects and electrothermal co-simulation of 3-D integrated packages.

Min Tang (M'09) was born in 1980. He received the B.S. degree in electronic engineering from Northwestern Polytechnical University, Xi'an, China, in 2001, the M.S. degree in electrical engineering from Xi'an Jiao Tong University, Xi'an, in 2004, and the Ph.D. degree in electronic engineering from Shanghai Jiao Tong University, Shanghai, China, in 2007.

Since 2007, he has been a faculty member with Shanghai Jiao Tong University, where he is currently an Associate Professor with the Department of Electronic Engineering. From 2010 to 2012, he was a Post-Doctoral Research Fellow with the University of Hong Kong, Hong Kong. His current research interests include modeling and simulation of high-speed interconnects, CAD of very large scale integration circuits, and computational electromagnetics.

Junfa Mao (M'92–SM'98–F'12) was born in 1965. He received the B.S. degree in radiation physics from the National University of Defense Technology, Changsha, China, in 1985, the M.S. degree in experimental nuclear physics from the Shanghai Institute of Nuclear Research, Chinese Academy of Sciences, Shanghai, China, in 1988, and the Ph.D. degree in electronic engineering from Shanghai Jiao Tong University, Shanghai, in 1992.

Since 1992, he has been a faculty member with Shanghai Jiao Tong University, where he is currently a Chair Professor and a Vice President. From 1994 to 1995, he was a Visiting Scholar with the Chinese University of Hong Kong, Hong Kong, and a Post-Doctoral Researcher with the University of California at Berkeley, Berkeley, CA, USA, from 1995 to 1996. He has authored or co-authored over 400 papers (including over 120 IEEE journal papers). His current research interests include the interconnect and package problems of integrated circuits and systems, and analysis and design of microwave components and circuits.